Global isochrons of a planar system near a phaseless set with saddle equilibria

James Hannam, Bernd Krauskopf, and Hinke M. Osinga

Department of Mathematics, The University of Auckland
Private Bag 92019, Auckland 1142, New Zealand

Abstract

Given an attracting periodic orbit of a system of ordinary differential equations, one can assign an asymptotic phase to any initial condition that approaches such a periodic orbit. All initial conditions with the same asymptotic phase lie on what is known as an isochron. Isochrons foliate the basin of attraction, and may have intriguing geometric properties. We present here two cases of a planar vector field for which the basin boundary — also referred to as the phaseless set — contains saddle equilibria and their stable manifolds. A continuation-based approach, in combination with Poincaré compactification when the basin is unbounded, allows us to compute isochrons accurately and visualise them as smooth curves to clarify their overall geometry.

1 Introduction

Many physical systems feature stable oscillations. One practical approach to studying such an oscillation is to apply a prescribed perturbation and record how the system returns to oscillatory behaviour. Of specific interest is the relative phase between the original stable oscillation and the oscillation to which the system settles down after the perturbation, which depends on when in the cycle the perturbation is applied. When the associated mathematical model is a system of ordinary differential equations, such an oscillation is represented by an attracting periodic orbit. The relative phase as a result of any perturbation can then be understood geometrically by considering what are known as the isochrons of the stable periodic orbit.

To introduce isochrons, we consider a system given by the vector field

$$\frac{d\vec{x}}{dt} = F(\vec{x}), \tag{1}$$

where $\vec{x} \in \mathbb{R}^n$, the function F is sufficiently smooth and the associated flow is denoted $\Phi(t, \vec{x_0})$. We suppose that system (1) has a (hyperbolic) attracting periodic orbit Γ of period T_Γ with basin of attraction $\mathcal{B}(\Gamma)$. We associate a phase with each point in Γ. By convention the point $\gamma_0 \in \Gamma$ with zero phase is chosen as the global maximum of Γ with respect to the first coordinate; the periodic orbit is then parametrised by the phase $\theta \in [0, 1)$ with $\gamma_\theta \in \Gamma$ defined by $\gamma_\theta = \Phi(\theta T_\Gamma, \gamma_0)$. We can then assign an asymptotic phase $\Theta : \mathcal{B}(\Gamma) \to [0, 1)$ to any point $\vec{x_0} \in \mathcal{B}(\Gamma)$ by the condition

$$\lim_{t\to\infty} \| \Phi(t, \vec{x_0}) - \Phi(t + \Theta(\vec{x_0})T_\Gamma, \gamma_0) \| = 0,$$

meaning that all points with the same phase $\Theta(\vec{x_0}) = \theta$ will synchronise with $\gamma_\theta \in \Gamma$.

In the 1970s, Arthur Winfree investigated the distribution of phase throughout the basin of attraction of oscillators of physical systems [14]. He coined the term isochron to describe the level sets of the asymptotic phase function Θ and he stated that these geometric objects are $(n-1)$-dimensional, unique, non-intersecting curves or surfaces inside the basin $\mathcal{B}(\Gamma)$. Moreover, Winfree observed that the isochrons accumulate on the basin boundary $\partial\mathcal{B}$, which he referred to as the phaseless set because this accumulation property makes it impossible to determine the phase of a point in $\partial\mathcal{B}$; see also the textbooks [2, 15]. The notion of an isochron was subsequently formalised in terms of dynamical systems theory by Guckenheimer [4]. The isochron $I(\gamma_\theta)$ is actually the stable manifold of the point $\gamma_\theta \in \Gamma$ under the time-T_Γ map $\Phi(T_\Gamma, \cdot)$. This point of view allowed Guckenheimer to prove properties of isochrons that were conjectured by Winfree in [14]. In particular, the set of isochrons

$$\mathcal{I}(\Gamma) = \{I(\gamma_\theta) \text{ for } \theta \in [0, 1)\}$$

is a foliation of $\mathcal{B}(\Gamma)$ by $(n-1)$-dimensional leaves over the (topological) circle Γ. Moreover, the flow is transverse to each isochron (i.e., leaf) $I(\gamma_\theta)$, which is also the diffeomorphic image of every other isochron in $I(\gamma_\psi)$ under the flow $\Phi((\theta - \psi)T_\Gamma, \cdot)$.

There has been a recent resurgence in the interest in isochrons, which has been motivated to a considerable extent by new methods of computing them. Huguet and Guillamon [5, 6] compute isochrons locally by making use of a functional equation, Osinga and Moehlis [11] and Langfield *et al.* [7] use a boundary value approach to compute isochrons of planar systems as curves parametrised by arclength, while Mauroy *et al.* [9] consider discretisations of the Koopman operator. Isochrons have been computed to investigate transient behaviour [1], to study their complicated geometry in slow-fast systems [7, 11], and to characterise the onset of phase sensitivity in terms of the loss of transversality of forward-time and backward-time isochrons [8].

As is the case in almost all literature on isochrons, we take the vector field (1) to be planar. In this case, the isochrons are smooth one-dimensional curves that foliate the two-dimensional basin $\mathcal{B}(\Gamma) \subset \mathbb{R}^2$. More specifically, we are concerned with the properties of isochrons near the basin boundary $\partial\mathcal{B}$. In the simplest case $\partial\mathcal{B}$ consist of a single repelling point, which directly implies that all the isochrons in $\mathcal{B}(\Gamma)$ accumulate on it. Slightly more complicated is the case that the basin boundary is formed by a repelling periodic orbit. Under the genericity condition that its period is different from T_Γ, all isochrons in $\mathcal{I}(\Gamma)$ accumulate on this periodic basin boundary; see [4] for the proof that, generically, the isochrons in $\mathcal{I}(\Gamma)$ accumulate on $\partial\mathcal{B}$.

The subject of this contribution is the question of how isochrons accumulate on a basin boundary that contains saddle equilibria. In this case $\partial\mathcal{B}$ is formed by the (closure of) stable invariant manifolds of the saddles. For the planar case considered here, the invariant manifolds are trajectories that converge to saddle equilibria, in forward time for a stable manifold $W^s(\cdot)$, and in backward time for an unstable manifold $W^u(\cdot)$. The invariant manifolds separate the plane into regions of qualitatively different behaviour. More specifically, the stable manifold $W^s(\cdot)$ of a saddle on the basin boundary acts as a separatrix for trajectories that converge to Γ and trajectories that do not. Hence, $W^s(\cdot)$ forms a part of $\partial\mathcal{B}$. Conversely, one branch of $W^u(\cdot)$ will converge to Γ and, thus, will intersect each isochron infinitely many times. Apart from these general statements, the overall geometry of isochrons in systems with basin boundaries formed by stable manifolds, especially in the case that they extend to infinity, has not been explored fully. Guckenheimer and Sherwood [13] study isochrons of a planar fast-slow system with a saddle point near a homolicinc bifurcation but do not consider the global geometry of the isochrons, Mauroy *et al.* [9] consider the local accumulation of isochrons along a stable manifold outside Γ, and likewise do not consider their global geometry. Finally, Shaw *et al.* [12]

briefly consider the isochrons of a piecewise linear system on a torus, where periodic orbits are separated by heteroclinic connections of invariant manifolds between saddle points.

In this paper we present the overall geometry of isochrons near the basin boundary $\partial\mathcal{B}$ for two cases that have not yet been investigated: firstly, for an unbounded basin $\mathcal{B}(\Gamma)$ in the form of a strip formed by two stable manifolds in $\partial\mathcal{B}$ that extend to infinity and, secondly, for a bounded component of $\partial\mathcal{B}$ consisting of the stable manifold of a single saddle whose two branches end at two repelling fixed points. To this end, we consider the planar vector field

$$\begin{cases} \dot{x} = \mu a\, x - y - b\, x(x^2 + y^2), \\ \dot{y} = x + \mu(a + c)\, y - (b + d)\, y(x^2 + y^2), \end{cases} \tag{2}$$

which we constructed as a modification of the Hopf normal form in the spirit of the example systems considered by Winfree [14] and Guckenheimer [4]. The origin $\mathbf{0}$ is always an equilibrium and system (2) is invariant under rotation by π; hence, all nonzero equilibria come in symmetric pairs. The effect of parameters c and d is to increase the velocity in the y-direction, where c has a greater affect near the origin, and d has a greater affect further away. Throughout, we fix $a = -0.1$, $b = 0.05$, $c = 0.9$ and $d = 0.45$, which allows us to study the isochrons of an attracting periodic orbit Γ for two different cases of phaseless sets with saddles by setting $\mu = 2.0$ and $\mu = 4.0$. We compute and present the relevant equilibria, their stable and unstable manifolds and a representative number of isochrons in $\mathcal{B}(\Gamma)$.

We show how isochrons in an unbounded basin can by computed reliably after Poincaré compactification of the plane, so that we can confirm and visualise their accumulation near infinity. For the case of a stable manifold of finite arclength inside Γ, we show how the isochrons spiral around and accumulate onto this type of component of $\partial\mathcal{B}$. Our findings agree with the theory, but we find that determining the precise geometry of isochrons in these situations is numerically very sensitive and presents considerable computational challenges. Throughout, we employ continuation of solutions of a suitably defined two-point boundary value problem to compute global isochrons accurately and efficiently as smooth curves paramaterised by arclength; see [7, 11] for more details of this approach.

2 Two phaseless sets generated by saddles

Figure 1 is the starting point of our investigation. It shows the phase portraits of system (2) for $\mu = 2.0$ and $\mu = 4.0$ in panels (a1) and (b1), respectively, consisting of the attracting periodic orbit Γ, repelling equilibria marked by squares and saddle equilibria marked by crosses, and their respective stable and unstable maniolds. Panels (a2) and (b2) additionally show ten isochrons that are uniformly distributed in phase θ, which is represented by colour as indicated in the colour bar.

In the phase portrait for $\mu = 2.0$ in Fig. 1(a1) the origin $\mathbf{0}$ is a source and forms the component of $\partial\mathcal{B}$ inside Γ. Outside Γ there are two saddle equilibria p^+ and p^-, which are counterparts under the symmetry of (2). Their stable manifolds $W^s(p^\pm)$ act as separatricies and, with the equilibria $p^\pm$, they form the outer part of $\partial\mathcal{B}$. Since $W^s(p^\pm)$ extend to infinity in the positive and negative y-directions, the basin $\mathcal{B}(\Gamma)$ is an unbounded vertical strip. The branches of the unstable manifolds $W^u(p^\pm)$ outside $\mathcal{B}(\Gamma)$ have no phase with respect to Γ as they extend to infinity in the positive and negative x-directions. The branches of $W^u(p^\pm)$ that lie inside $\mathcal{B}(\Gamma)$, on the other hand, converge to Γ, and thus each point in $W^u(p^\pm) \cap \mathcal{B}(\Gamma)$ has a phase. This means that each isochron of Γ must intersect $W^u(p^\pm)$ infinitely many times; in particular, since $W^u(p^\pm)$ converge to $p^\pm$ in backward time, the isochrons must accumulate on $W^s(p^\pm)$ near $p^\pm$.

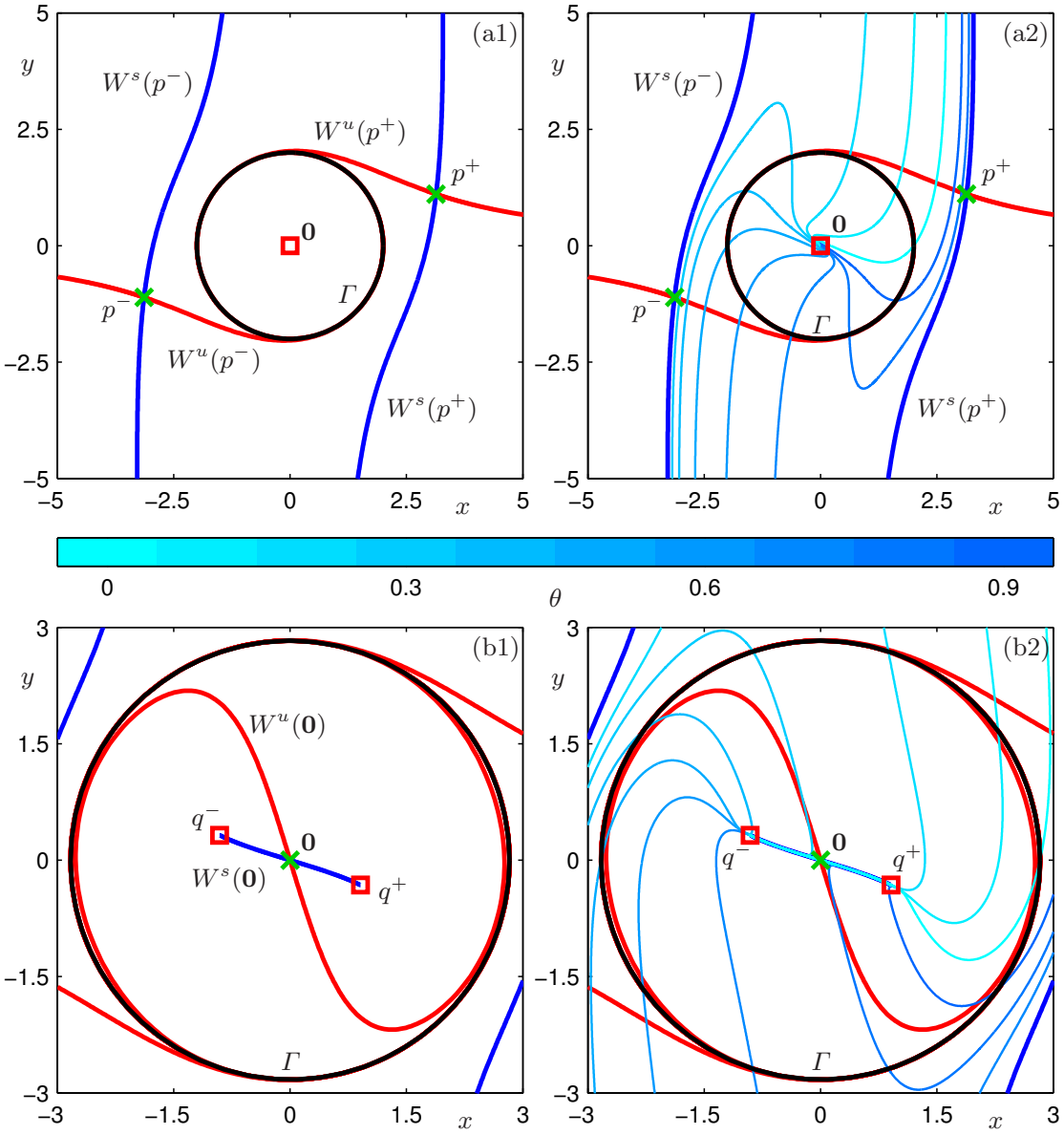

Figure 1: Phase portraits and isochrons of (2) for $\mu = 2$ in row (a) and for $\mu = 4$ in row (b). Shown are the periodic orbit Γ (black), equilibria (green crosses for saddles, and red squares for sources), and the stable (blue) and unstable (red) manifolds of the saddle equilibria. The right column also shows ten isochrons that are distributed uniformly in phase θ along Γ, where colour indicates the phase according to the central colour bar.

Figure 1(a2) shows the same phase portrait but with ten isochrons, which are equally distributed in asymptotic phase and coloured according to the colour bar. Inside Γ the isochrons simply accumulate on the source $\mathbf{0} \subset \partial\mathcal{B}$. On the outside of Γ, and beyond its immediate vicinity, we observe that each isochron intersects the unstable invariant manifold $W^u(\cdot)$ of either p^+ or p^- once, but then appears to run parallel to the respective branch of $W^s(p^\pm)$ and extends out of the frame. We computed these ten isochrons up to excessively large arclength, yet they do not appear to turn around and come back into the frame, near the other saddle equilibrium, to intersect $W^u(p^\pm)$ again. Hence, the isochrons in Fig. 1(a2) do not appear to accumulate on $\partial\mathcal{B}$, which would contradict the theory. The issue is the extreme growth towards infinity of the isochrons of system (2) in the unbounded strip $\mathcal{B}(\Gamma)$, which we will address and solve in Sec. 3 by means of Poincaré compactification.

Figure 1(b1) is the phase portrait for $\mu = 4.0$, where we now concentrate on the component of $\partial\mathcal{B}$ inside Γ; the phase portrait outside Γ is topologically as that for $\mu = 2.0$ in panel (a1). As panel (b1) illustrates, the origin $\mathbf{0}$ is now a saddle point. In fact, two sources $q^\pm$ have bifurcated from $\mathbf{0}$ in a pitchfork bifurcation at $\mu \approx 3.5355$, and the two branches of the stable manifold $W^s(\mathbf{0})$ converge in backward time to q^+ and q^-. Note that $W^s(\mathbf{0})$ is a curve of finite arclength; its closure, which includes $\mathbf{0}$ and $q^\pm$, forms the component of $\partial\mathcal{B}$ inside Γ. The unstable manifold $W^u(\mathbf{0})$ lies entirely inside $\mathcal{B}(\Gamma)$, and its to branches converge to Γ very rapidly in forward time. Therefore, each point in $W^u(\mathbf{0})$ has a phase and each isochron of Γ must intersect each of the two (symmetrically related) branches of $W^u(\mathbf{0})$ infinitely many times; hence, the isochrons must accumulate on $W^s(\mathbf{0})$ near $\mathbf{0}$.

Figure 1(b2) shows the phase portrait and additionally ten isochrons uniformly distributed in phase. Inside Γ the isochrons indeed approach $W^s(\mathbf{0})$ very rapidly, and it unclear how exactly they approach the inner component of $\partial\mathcal{B}$. Moreover, it seems from this figure that outside some neighbourhood of Γ each isochron intersects $W^u(\mathbf{0})$ only once, which is due to very strong contraction towards $\mathbf{0}$ along $W^u(\mathbf{0})$. In fact, the isochrons quickly reach a distance to $W^s(\mathbf{0})$ that is on the order of the computational accuracy. The accumulation of isochrons on the component of $\partial\mathcal{B}$ in the region enclosed by Γ is detailed and illustrated in Sec. 4.

3 The geometry of isochrons near infinity

The issue with the phase portrait and ischrons of (2) for $\mu = 2.0$ in Figure 1(a2) is that the basin of attraction $\mathcal{B}(\Gamma)$ extends to infinity in the positive and negative y-directions while it is bounded in the x-direction. This means that isochrons make long excursion in the y-direction before returning back to the region of interest near the origin; in fact, the isochrons would need to be computed for impractically large arclengths in the state space $\mathbb{R}^2$ of (2) to show them returning. Since (2) is a polynomial vector field, this issue can be addressed effectively by means of Poincaré compactification; see for example [3, 10]. For the planar case considered here, the idea is to map $\mathbb{R}^2$ diffeomorphically to the open unit disk $\mathbb{D}^2$, where the circle $\partial\mathbb{D}^2 = \mathbb{S}^1$ represents the directions of approach to, or departure from infinity. The transformed vector field on $\mathbb{D}^2$ is then conjugate to the original vector field on $\mathbb{R}^2$ and, moreover, it is continuous on the closed disk $\mathbb{D}^2 \cup \mathbb{S}^1$ after an appropriate rescaling of time. In particular, the phase portrait as well as the isochron structure remain qualitatively the same. However, as we will see, isochrons of (2) that approach infinity can be computed efficiently as curves in the new coordinates because arclength is now measured in the bounded space $\mathbb{D}^2$.

Geometrically, the transformation is best described in two steps. Consider the unit sphere $\mathbb{S}^3$ in $\mathbb{R}^3$, centred at the origin $(0, 0, 0)$, and the plane $\mathbb{R}^2 \cong \{(x, y, z) \in \mathbb{R}^3 \text{ with } z = 1\}$, which is tangent to $\mathbb{S}^3$ at its north pole $(0, 0, 1)$. The first coordinate transformation projects the point $(x, y, 1) \in \mathbb{R}^2$ to a point (s_1, s_2, s_3) on, say, the upper half-sphere of $\mathbb{S}^3$ by determining

the intersection point of the line through $(x, y, 1)$ and $(0, 0, 0)$ with $\mathbb{S}^3$ where s_3 is positive; the equator of $\mathbb{S}^3$ then represents the asymptotic directions (of trajectories) at infinity. The second step is the projection of the closed upper half-sphere (that is, including the equator) back to the plane $\mathbb{R}^2$ by considering its intersection point with the line through the given point $(s_1, s_2, s_3) \in \mathbb{S}^3$ and the south pole $(0, 0, -1)$. The image is the closed disk of radius 2 which is scaled to $\mathbb{D}^2$. The overall coordinate transformation from $(x, y) \in \mathbb{R}^2$ to the $(u, v) \in \mathbb{D}^2$ is given by

$$\begin{bmatrix} u \\ v \end{bmatrix} = \frac{1}{1 + \sqrt{x^2 + y^2 + 1}} \begin{bmatrix} x \\ y \end{bmatrix}, \tag{3}$$

and its inverse by

$$\begin{bmatrix} x \\ y \end{bmatrix} = \frac{2}{1 - u^2 - v^2} \begin{bmatrix} u \\ v \end{bmatrix}. \tag{4}$$

Transforming an actual planar vector field requires multiplication of the right-hand side by the Jacobian of the coordinate transformation (3). This generally results in the transformed vector field being singular on $\partial\mathbb{D}^2 = \mathbb{S}^1$; for polynomial vector fields this issue can be dealt with by desingularisation in the form of a time rescaling with $s_3^n = \left(\frac{1-u^2-v^2}{1+u^2+v^2}\right)^n$, where n is the (highest) order of the polynomial vector field.

For the specific case of (2), the compactified vector field on $\mathbb{D}^2 \cup \mathbb{S}^1$, written as a matrix-vector product, takes the form:

$$\begin{aligned} \begin{bmatrix} \dot{u} \\ \dot{v} \end{bmatrix} = & \frac{1}{(1 + u^2 + v^2)^3} \begin{bmatrix} 1 + v^2 - u^2 & -2uv \\ -2uv & 1 + u^2 - v^2 \end{bmatrix} \\ & \begin{bmatrix} (1 - u^2 - v^2)^2 (\mu a\, u - v) - 4b\, u(u^2 + v^2) \\ (1 - u^2 - v^2)^2 (u + \mu(a + c)\, v) - 4(b + d)\, v(u^2 + v^2) \end{bmatrix}. \end{aligned} \tag{5}$$

The phase portrait on $\mathbb{D}^2$ of (5) for $\mu = 2$ is shown in Fig. 2(a). Indeed, it features qualitatively the same, although transformed, invariant objects found in the phase portrait of (2), shown in row (a) of Fig. 1; for simplicity, we refer to these also as Γ, $\mathbf{0}$, $p^{\pm}$, $W^s(p^{\pm})$ and $W^u(p^{\pm})$. Also shown in Fig. 2(a) is the circle $\mathbb{S}^1$, which is invariant and represents the asymptotic directions of trajectories at infinity. There are four equilibria on $\mathbb{S}^1$, two sinks $s_\infty^{\pm}$ at $(u, v) = (\pm 1, 0)$ onto which the respective branches of $W^u(p^{\pm})$ converge, and two sources $q_\infty^{\pm}$ at $(u, v) = (0, \pm 1)$ onto which the respective branches of $W^s(p^{\pm})$ converge in backward time. In particular, $\mathcal{B}(\Gamma)$ is the compact region bounded on the outside by $W^s(p^{\pm}) \cup p^{\pm} \cup q_\infty^{\pm}$, which is the closure of $W^s(p^{\pm})$. Also shown in Fig. 2(a) are the same (but transformed) ten isochrons from Fig. 1(a2). Inside Γ, the compactification has little effect. On the other hand, as Fig. 2 shows clearly, their properties near the outside component of $\partial\mathbb{B}$ now become apparent. Outside Γ, all isochrons accumulate on $\partial\mathbb{B}$ in a spiralling fashion, and in this way each isochron, indeed, intersects $W^u(p^{\pm})$ infinitely often near $p^{\pm}$. The close passage of the isochrons near q_∞^- is illustrated in Fig. 2(b).

As Fig. 2 clearly shows, Poincaré compactification allows us to determine and illustrate the geometry of the isochrons globally throughout an entire basin $\mathcal{B}(\Gamma)$ that is unbounded. Note that each isochron of (5) has maxima and minima in v at successively larger $|v|$-values, but these are bounded by 1. By contrast, in the original coordinates of (2), the arclength of the isochrons up to the second maximum or minimum is already prohibitively large; this is why Fig. 2(b2) does not show the computed isochrons returning. After Poincaré compactification, on the other hand, the isochrons are confined to a bounded region, and this makes it possible to compute them efficiently as global parametrised curves.

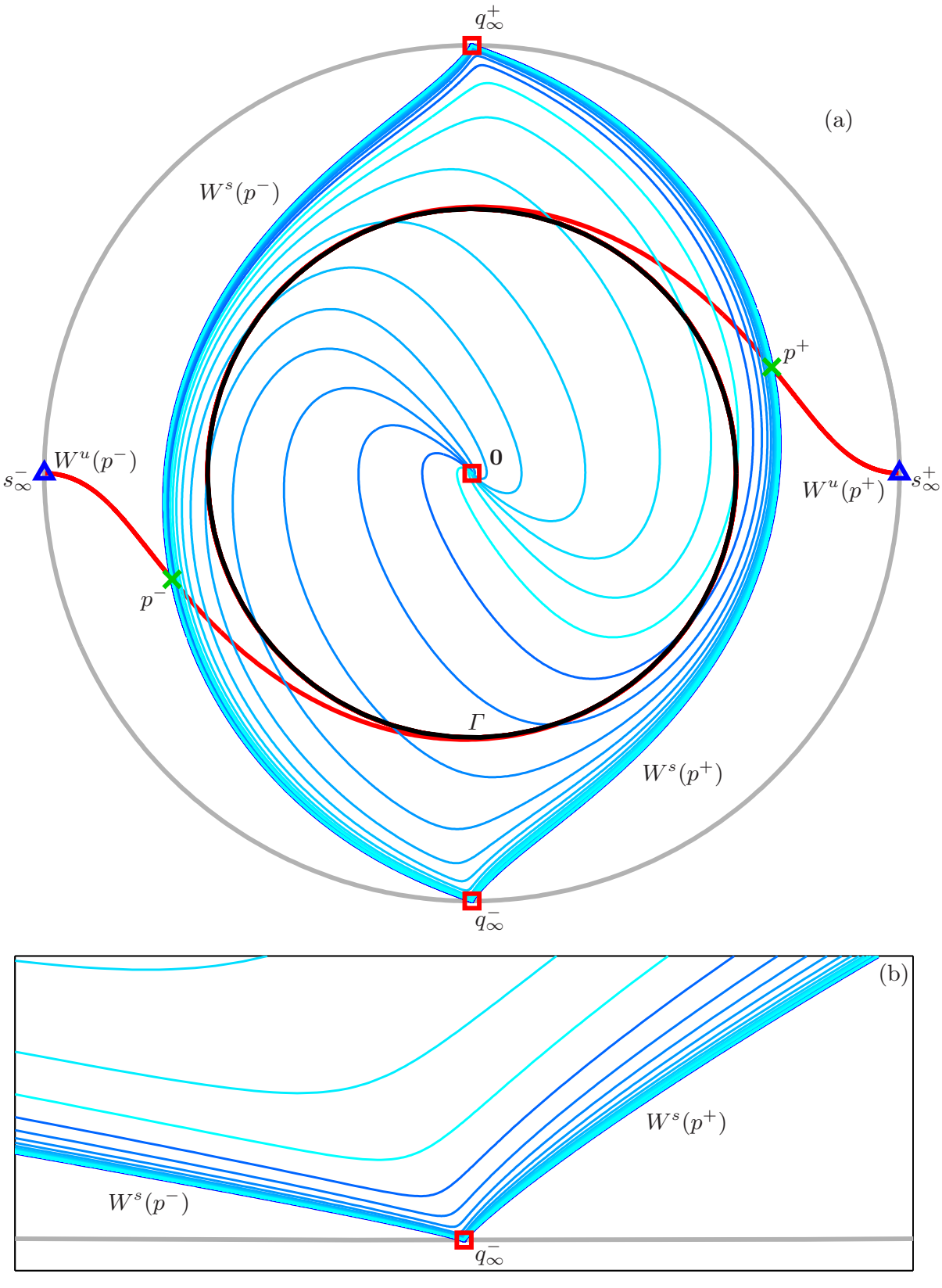

Figure 2: Accumulation on $\partial\mathcal{B} \subset \mathbb{D}^2 \cup \mathbb{S}^1$ of isochrons of (5) for $\mu = 2$. Shown are Γ (black), **0** (red square), $p^\pm$ (green crosses), $W^s(p^\pm)$ (blue) and $W^u(p^\pm)$ (red), the unit circle $\mathbb{S}^1$ (grey), representing the asymptotic directions of trajectories at infinity, with sinks $s^\pm_\infty$ at $(u, v) = (\pm 1, 0)$ (blue triangles) and sources $q^\pm_\infty$ at $(u, v) = (0, \pm 1)$ (red squares), and ten isochrons distributed uniformly in phase θ (shades of blue). Panel (a) shows all of $\mathbb{D}^2 \cup \mathbb{S}^1$ and should be compared with Fig. 1(b), while panel (b) is a enlargement near q^-_∞.

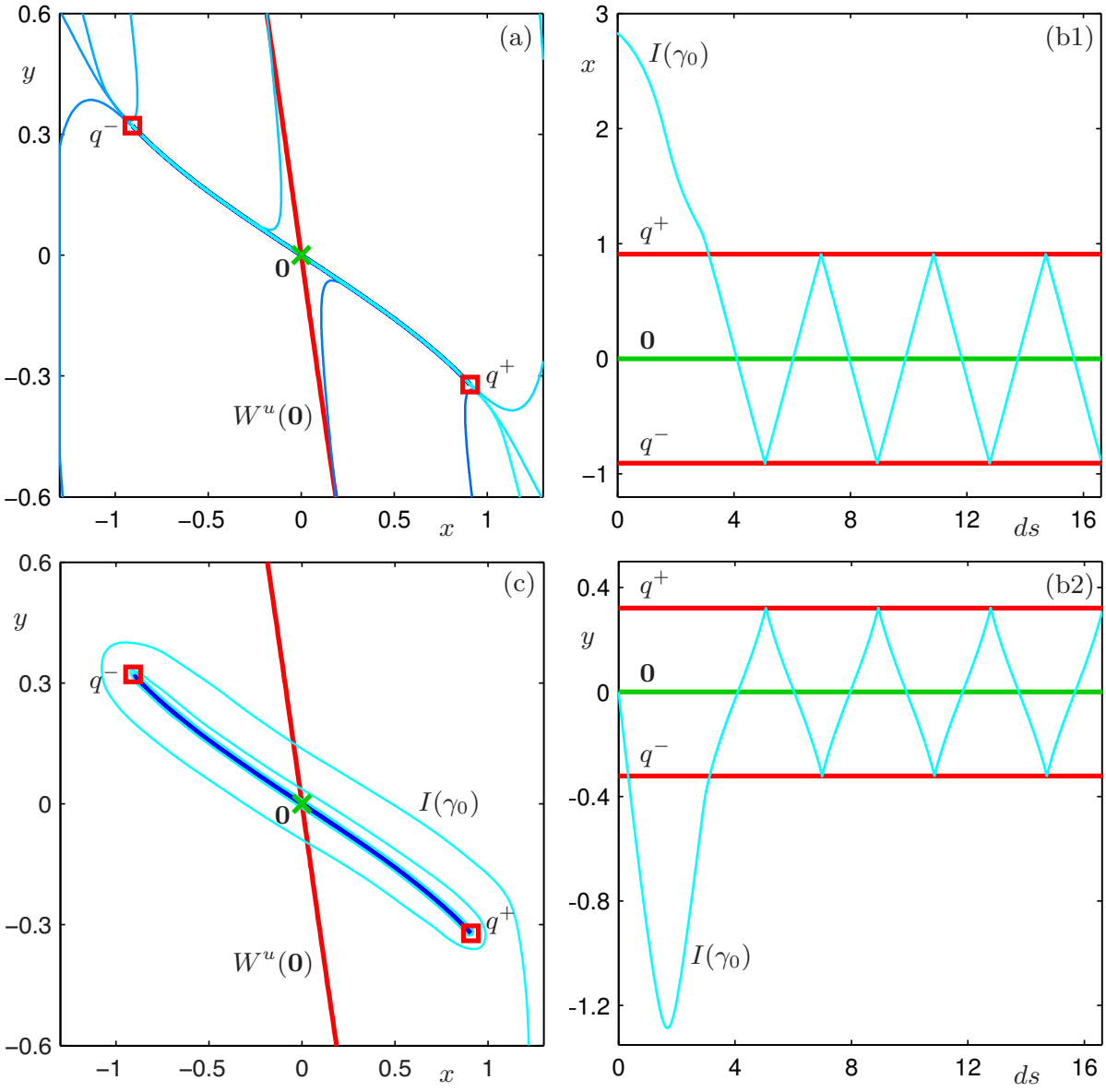

Figure 3: Accumulation on $\partial\mathcal{B}$ of isochrons of (2) for $\mu = 4$. Panel (b1) shows the very rapid accumulation onto $W^s(\mathbf{0}) \cup \mathbf{0} \cup q^{\pm}$ of ten isochrons that are uniformly distributed in phase. Panels (a1) and (a2) show the x- and y-components of $I(\gamma_0)$ against its arclength ds; also shown are the respective components of $\mathbf{0}$ (green line) and $q^{\pm}$ (red line). Panel (b2) is a sketch of how $I(\gamma_0)$ spirals onto $\partial\mathcal{B}$.

4 The geometry of isochrons near $W^s(\mathbf{0})$

We now return to the question of how the isochrons of (2) for $\mu = 4$ accumulate on the component $W^s(\mathbf{0}) \cup \mathbf{0} \cup q^{\pm}$ of $\partial\mathcal{B}$ inside Γ. Figure 3(a) illustrates that the isochrons, of which again ten are shown, accumulate on $\partial\mathcal{B}$ so rapidly that they lie less that the computational tolerance of 10^{-8} from $W^s(\mathbf{0}) \cup \mathbf{0}$ within one revolution after passing $\mathbf{0}$ closely for the first time. This is owing to the fact that the expansion along the unstable direction over one period of Γ is of the order $e^{\lambda_u T_\Gamma} \approx 8 \times 10^7$, where λ_u is the unstable eigenvalue of $\mathbf{0}$. We remark that

such rapid accumulation of isochrons on a stable manifold must be regarded as not so unusual, because it arises from the fact that the period T_Γ is generally reasonably large; hence, consecutive intersection points of an isochron with the same branch of $W^u(\mathbf{0})$ converge to $\mathbf{0}$ at a very fast rate, even when λ_u is only of moderate magnitude.

This explains why it is not possible to visualise the accumulation of the isochrons in Fig. 3(a). To determine its exact nature, column (b) of Fig. 3 shows the x- and y-components of points on $I(\gamma_0)$ plotted as a function of the arclength ds along $I(\gamma_0)$ measured from γ_0. The equilibria $\mathbf{0}$ and $q^\pm$ are shown as labelled horizontal lines, which allow us to see that $I(\gamma_0)$ oscillates between q^+ and q^- in both the x-component and the y-component. Taken together, panels (b1) and (b2) are evidence that $I(\gamma_0)$ spirals around $W^s(\mathbf{0}) \cup \mathbf{0} \cup q^\pm$ and, hence, intersects both branches of $W^u(\mathbf{0})$ infinitely often in the process. To illustrate what this looks like qualitatively in the (x, y)-plane of (2), Fig. 3(c) shows $\mathbf{0}$, $q^\pm$, $W^s(\mathbf{0})$ and $W^u(\mathbf{0})$ overlaid with a sketch of $I(\gamma_0)$. This sketch is based on the evidence in panels (b1) and (b2), and can be interpreted as a rescaling of the vector field along the direction of the unstable eigenvector.

5 Conclusion

We have investigated the geometry of isochrons in a planar system as they accumulate on a basin boundary that is formed by the stable manifolds of saddle equilibria. As theory states, the isochrons accumulate (generically) on such a boundary and we investigated how this happens geometrically. We considered first the case of an unbounded basin formed by the stable manifolds of two saddles. In the original coordinates it is practically impossible to compute and visualise the accummulation of the isochrons on such a boundary. After Poincaré compactification of the vector field, on the other hand, the isochrons can be computed readily and the accummulation becomes apparent. We also considered a component of the basin boundary consisting of the stable invariant manifold of a saddle of finite arclength that begins at two repellors. The isochrons can be computed in this case, but the issue is that their accumulation onto this type of boundary is very rapid. Nevertheless, we were able to show how they spiral around the boundary, intersecting the unstable manifold of the saddle infinitely many times in the process.

We presented here two case studies of how isochrons may accummulate on the boundary of the basin of attraction — the phaseless set. There are other, qualitatively different possibilities for what a component of the boundary of a basin of attraction of a planar vector field may look like. Different cases will be addressed in the same spirit, by a combination of two-point boundary value problem methods and Poincaré compactification. Ongoing research will also consider the foliation by one-dimensional isochrons of the stable and unstable manifolds of a saddle periodic orbit of a vector field in $\mathbb{R}^3$. There are interesting possibilities for these invariant objects to interact, for example, along homoclinic orbits.

The next challenge will then be the computation of two-dimensional isochrons of an attracting periodic orbit in $\mathbb{R}^3$ as invariant manifolds. This will allow the investigation of the geometry of two-dimensional isochrons that foliate the basin of attraction; this geometry is expected to be much more complex, given the multitude of dynamics that one may find in a three-dimensional state space. In particular, the question will again be how isochrons accumulate on the basin boundary, which may include saddle equilibiria, saddle periodic orbits and their stable manifolds. The latter may extend to infinity or accummulate on other invariant sets. Poincaré compactification of $\mathbb{R}^3$ to the inside of a sphere will be crucial for studying the geometry of two-dimensional isochrons globally.

Acknowledgements

We thank Peter Langfield for his advice regarding the computations of isochrons and Andrus Giraldo for helpful discussions on Poincaré compactification.

References

[1] O. Castejón, A. Guillamon, and G. Huguet. Phase-amplitude response functions for transient-state stimuli. *The Journal of Mathematical Neuroscience*, 3:1–26, 2013.

[2] L. Glass and M.C. Mackey. *From Clocks to Chaos*. Princeton, 1988.

[3] E.A. González Velasco. Generic properties of polynomial vector fields at infinity. *Transactions of the American Mathematical Society*, 143:201–222, 1969.

[4] J. Guckenheimer. Isochrons and phaseless sets. *Journal of Mathematical Biology*, 1(3):259–273, 1975.

[5] A. Guillamon and G. Huguet. A computational and geometric approach to phase resetting curves and surfaces. *SIAM Journal on Applied Dynamical Systems*, 8(3):1005–1042, 2009.

[6] G. Huguet and R. de la Llave. Computation of limit cycles and their isochrons: fast algorithms and their convergence. *SIAM Journal on Applied Dynamical Systems*, 12(4):1763–1802, 2013.

[7] P. Langfield, B. Krauskopf, and H.M. Osinga. Solving Winfree's puzzle: The isochrons in the FitzHugh-Nagumo model. *Chaos: An Interdisciplinary Journal of Nonlinear Science*, 24(1):013131, 2014.

[8] P. Langfield, B. Krauskopf, and H.M. Osinga. Forward-time and backward-time isochrons and their interactions. *SIAM Journal on Applied Dynamical Systems*, 14(3):1418–1453, 2015.

[9] A. Mauroy, B. Rhoads, J. Moehlis, and I. Mezic. Global isochrons and phase sensitivity of bursting neurons. *SIAM Journal on Applied Dynamical Systems*, 13(1):306–338, 2014.

[10] M. Messias. Dynamics at infinity and the existence of singularly degenerate heteroclinic cycles in the Lorenz system. *Journal of Physics A: Mathematical and Theoretical*, 42(11):115101, 2009.

[11] H.M. Osinga and J. Moehlis. Continuation-based computation of global isochrons. *SIAM Journal on Applied Dynamical Systems*, 9(4):1201–1228, 2010.

[12] K.M. Shaw, Y.-M. Park, H.J. Chiel, and P.J. Thomas. Phase resetting in an asymptotically phaseless system: On the phase response of limit cycles verging on a heteroclinic orbit. *SIAM Journal on Applied Dynamical Systems*, 11(1):350–391, 2012.

[13] W.E. Sherwood and J. Guckenheimer. Dissecting the phase response of a model bursting neuron. *SIAM Journal on Applied Dynamical Systems*, 9(3):659–703, 2009.

[14] A.T. Winfree. Patterns of phase compromise in biological cycles. *Journal of Mathematical Biology*, 1(1):73–93, 1974.

[15] A.T. Winfree. *The Geometry of Biological Time*. Springer-Verlag, 1980.